Stopped-Flow Studies of the Reduction of the Copper Centers Suggest a Bifurcated Electron Transfer Pathway in Peptidylglycine Monooxygenase[†]

Shefali Chauhan[‡], **Parisa Hosseinzadeh**[§], **Yi Lu**[§], and **Ninian J. Blackburn**[*,‡]

Institute of Environmental, Health, Oregon Health and Science University, 3181 SW Sam Jackson Park Road, Portland, OR 97239, and Department of Chemistry and Biochemistry, University of Illinois Urbana-Champaign, 600 S Mathews Ave, Urbana, IL 61801

Abstract

PHM is a dicopper enzyme that plays a vital role in the amidation of glycine extended pro-peptides. One of the crucial aspects of its chemistry is the transfer of two electrons from an electron-storing and transferring site (CuH) to the oxygen binding site and catalytic center (CuM) over a distance of 11 Å during one catalytic turnover event. Here we present our studies on the first electron transfer step (reductive phase) in the WT PHM as well as its variants. Stopped-flow was used to record the reduction kinetic traces using the chromophoric agent DMPD as the reductant. The reduction was found to be biphasic in the WT PHM with an initial fast phase ($17.2s^{-1}$) followed by a much slower phase ($0.46s^{-1}$). We were able to ascribe the fast and slow phase to the CuH and CuM-sites respectively by making use of the H242A and H107H108A mutants which only contain the CuH-site and CuM-site respectively. In the absence of substrate the redox potentials determined by cyclic voltammetry were 270 mV (CuH-site) and −15 mV (CuM-site), but binding of substrate (Ac-YVG) was found to alter both potentials so that they converged to a common value of 83 mV. Substrate binding also accelerated the slow reductive phase by ~10 fold, an effect that could be explained at least partially by the equalization of the reduction potential of the copper centers. Studies on H108A showed that the ET to the CuM-site is blocked, highlighting the role of the H108 ligand as a component of the reductive ET pathway. Strikingly, the rate of reduction of the H172A variant was unaffected despite the rate of catalysis being three orders of magnitude less than that of the WT PHM. These studies strongly indicate that the reductive phase and catalytic phase ET pathways are different and suggest a bifurcated ET pathway in PHM. We propose that H172 and Y79 form part of an alternate pathway for the

[*]To whom correspondence should be addressed. N.J.B Phone: (503) 346-3428 Fax: (503) 346-3427. ; Email: blackbni@ohsu.edu
[‡]Oregon Health & Sciences University
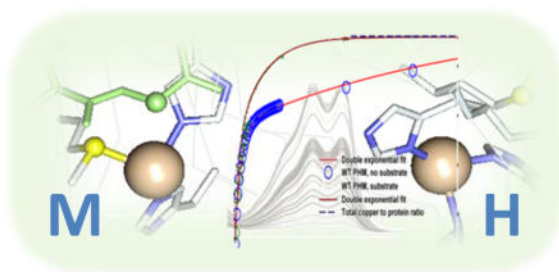[§]University of Illinois

catalytic phase ET while the H108 ligand along with the water molecules and substrate form the reductive phase ET pathway.

Graphical abstract

Amidation is a post-translational modification required for the bioactivation of glycine-extended pro-peptides (1–3) which are components of essential signaling pathways (3–5). The reaction is catalyzed by the bifunctional enzyme peptidylglycine α-amidating monooxygenase (PAM), and involves addition of an amide group to the C-terminus of a glycine extended pro-peptide substrate (6, 7). Amidation proceeds in two sequential steps each catalyzed by individual domains of the PAM enzyme : hydroxylation, catalyzed by the copper-containing peptidylglycine α-hydroxylating monooxygenase (PHM) and dealkylation of the carbinolamide intermediate catalyzed by the Ca/Zn containing peptidylglycine α-amidating lyase (PAL) (8, 9). Specifically, the PHM domain mediates the stereospecific hydroxylation of the terminal glycine of the peptide substrate to form a peptidyl-α-hydroxyglycine intermediate which undergoes N-C bond fission and elimination of glyoxalate to yield the α-amidated product (10–12) (Figure 1).

PHM belongs to the family of type 2 copper containing monoxygenases, which also includes its homologues, dopamine β-monoxygenase (DBM) (13) and tyramine β-monooxygense (TBM) (14, 15). PHM is a di-copper containing enzyme (16, 17) composed of two domains (18), with each domain housing a copper center, separated by an 11 Å water-filled cleft (3, 19, 20). The copper centers, termed CuH and CuM are functionally inequivalent and differ in geometry as well as the set of ligands (21, 22). The CuH site is ligated to Nδ of three histidines (H107, H108 and H172), whereas the CuM site is bound by the Nε of two histidines (H242, H242) and the sulfur of methionine (M314) (3, 19, 20). The CuM site serves as the oxygen binding and catalytic site and a pre-catalytic dioxygen-bound state has been described by crystallography (23). The CuH site is believed to be involved in electron transfer (ET) (3, 20, 24–27).

During each catalytic turnover event, the Cu(II)H and Cu(II)M sites of the enzyme are reduced by the physiological reductant ascorbate to form Cu(I)H and Cu(I)M (28–30). This is the active state of the enzyme, which reacts via equilibrium-ordered binding of first peptide substrate and then dioxygen to form an E•S•O_2 ternary complex (31, 32). The committed step in the enzyme reaction mechanism involves extraction of an electron from the M-site to form a superoxo intermediate (Cu(II)M-O_2-) (24–26, 33, 34) which is most likely bound end-on and protonated (35). This is sufficiently electrophilic to abstract a pro-S

hydrogen atom from the substrate by a hydrogen tunneling mechanism (31, 36) thereby forming peroxide and a substrate radical. Hydroxylation is believed to be accomplished by peroxide O-O bond cleavage and radical rebound to the substrate radical in a step of low activation energy, which also includes the transfer of a second electron from CuH to CuM.

Among many aspects of PHM chemistry that remain elusive, the ET from H-site to the M-site is one of the most challenging. The two electrons required for substrate hydroxylation are delivered to the catalytic M-site at different stages of the reaction cycle. The first electron reduces the Cu(II)M species to the Cu(I)M state in a step we call the "reductive" ET phase prior to binding of dioxygen at M. The second electron is transferred in a step we call the oxidative or "catalytic" ET phase after the enzyme has committed to catalysis, and is generally believed to reduce a high-valent species such as Cu(III)=O or Cu(II)-O• formed after the O-O bond has broken. It has been proposed (25) that the spatial separation between the two coppers prevents fast ET from the CuH center thereby amplifying the reactivity of the CuM-superoxo species, but the enzyme pays an energetic price for the increased oxygen reactivity by necessitating long range electron transfer from CuH to CuM. Although the intersite distance is consistent with fast ET (37), the open access of solvent to both copper centers, and the large coordination changes that accompany reduction to Cu(I) (22) have raised intriguing questions as to how the enzyme avoids the associated unfavorable reorganizational energies. A number of proposals for the catalytic ET step have been advanced. These have included superoxide channeling (38); a "substrate-mediated" pathway involving H108, Q170, a water molecule, and the peptide substrate; direct interaction of the Cu(I)H with the substrate radical via domain movement (39); and transfer across the inter-site cavity via an ordered array of water molecules, perhaps assisted by Y79 (26, 27, 40). However, these mechanisms do not account for all of the available data. For example, the superoxide channeling theory predicts superoxide leakage, but none has been detected - instead the reduction of oxygen and substrate hydroxylation remained completely coupled even in the presence of slow substrates and variants of low catalytic activity (26, 41, 42). Similarly, mutation of the critical substrate-mediated pathway residue Q170 has only limited effects on the steady state kinetics (43). Thus, none of these theories are able to fully explain all aspects of the ET.

In an effort to investigate further the important elements of the ET process, we have used stopped-flow spectrophotometry to measure the rates of reduction of the H- and M-sites in the oxidized state of the WT enzyme and important semi-functional variants. Cyclic voltammetry studies have also been undertaken in a bid to understand the significance of the reduction potential of copper centers in defining their individual roles. Our results show that the reductive event is biphasic, with a fast step followed by a much slower one. The binding of substrates (Ac-YVG, hippuric acid and nitrohippuric acid) leads to a dramatic acceleration of the slow reductive step, associated with an increase in the reduction potential of one of the copper centers. Studies on the single-site mutants H107H108A (M-site occupied, H-site empty) and H242A (H-site occupied, M-site empty) (44) have allowed assignment of fast and slow rates of reduction to the H- and M-site respectively. The role of the histidine ligands of the H-site was investigated by performing reduction kinetics on mutants in which each histidine was mutated to alanine (H107A, H108A, and H172A). The results suggested that H108 is the most important component of the reductive ET pathway

implying that it may serve as a unique conduit for H to M electron transfer. On the other hand, despite its profound effect on the rate of H-atom abstraction (41) H172 appeared to be unimportant for reductive ET. These data have led to the conclusion that the pathways for reductive and oxidative ET may be bifurcated, with the reductive electron following a different path from the oxidative electron. Implications for the enzymatic mechanism are discussed.

Materials and Methods

Buffers, ascorbate, N, N-dimethyl-p-phenylenediamine dihydrochloride (DMPD) were obtained from Sigma-Aldrich at a minimum purity of 99%. The substrate Ac-Tyr-Val-Gly (Ac-YVG) was purchased from Peptide International. Hippuric acid and nitrohippuric acid were purchased from Sigma-Aldrich.

Construction of variants

WT PHM catalytic core (PHMcc, residues 42–356) and its variants H107A, H172A and H242A were constructed as described previously (17). For H108A and H107H108A, constructs carrying the mutations were individually introduced into pBS. ProPHM382s (obtained as a gift from Betty A. Eipper and Richard E. Mains) using Splicing by Overlap Extension (SOEing) also as described previously (44). CHO DG44 cells were transfected with the recombinant DNA using Lipofectamine 2000 (Invitrogen). The transfected cells were subsequently selected for *Dhfr* cell lines in α-minimum Eagle's medium (MEM) containing 10% dialyzed fetal bovine serum. Only those cells that retained the *Dhfr* gene (co-located with PHM on the plasmid) were capable of growth under these conditions. Monoclonal cell lines were created by serial dilution into 96-well plates in order to select for wells which contained single cell colonies. These were passed individually into a fresh 96 well, grown to confluence, and screened via western blot for PHMcc production under similar conditions. The strongest producers were inoculated into a Hollow Fiber Bioreactor with 5 MWCO (Fibercell Systems, Inc.).

Western Blot Analysis

CHO DG44 cells were incubated in DMEM/F12 media containing 0.5% Fetal Clone II (FCII, Fisher) for at least 24h before a sample was collected. The sample was mixed with SDS and heated for 5 minutes at 100°C. Each sample was separated on an 8–25% SDS-PAGE and then transferred to an Immobilon P membrane (Millipore) using the PhastSystem (Applied Biosciences). PHM proteins were visualized using rabbit antibody 246 [rPAM (116–131)] (7) diluted 1:1500, and secondary antibody-antirabbit IgG (Sigma) diluted 1:1000, followed by an AP Conjugate Substrate Kit (Bio-Rad Laboratories).

PHM Expression and Purification

The stably transfected cell lines were thawed from freezer stock into a T75 flask with 20mL of DMEM/F12 medium containing 10% FCII serum (Fisher). At 80% confluence, the cells were passed into five NUNC triple flasks (500cm^2 per flask) which were also grown to confluence. The cells were trypsinized and re-suspended in 50 mL DMEM/F12 medium with 10% FCII serum prior to inoculation into the extra-capillary space (ECS) of a Hollow

Fiber Bioreactor (Fibercell Systems 4300-C2008, MWCO 5kD, 3000cm^2 surface area) pre-cultured with 2L of 50mM PBS pH 7.35 and 2L of DMEM/F12 10% FCII serum (22, 38, 45). Individual bioreactors containing each of the variants were fed with DMEM/F12/10% FCII serum for a month. The serum level was then reduced to 0.5%, at which point spent medium (20mL) from the ECS was collected every other day and frozen at −20°C for later purification. About a month worth of the bioreactor harvest (300mL) for each variant was purified as previously described (22, 38, 45).

PHM Copper Reconstitution

For WT PHM, H107A, H108A and H172A, purified enzyme was dialyzed against 20mM sodium phosphate buffer, pH 8.0 and then reconstituted with 2.5 mole equivalents cupric sulfate per protein followed by two cycles of dialysis to remove unbound cupric ions. For the single-site variants (H107H108A and H242A), the purified protein was initially dialyzed against 20mM sodium phosphate buffer, pH 8.0 overnight, reconstituted with 2.5 equivalents of cupric sulfate using a syringe pump, at a rate of 60ul/hr, and dialyzed exhaustively against copper-free phosphate buffer at the same pH and ionic strength. This procedure resulted in copper to protein ratios close to 1. Thereafter, the single-site mutants were reconstituted with 1.3 equivalents of cupric sulfate, and dialyzed overnight against 20mM sodium phosphate buffer, pH 8. Protein concentration was determined by O.D$_{280}$ on a Cary-50 UV-vis spectrophotometer at room temperature using an extinction coefficient for a 1% solution at 280nm of 0.980. The copper concentrations were determined using a Perkin-Elmer Optima 2000 DV inductively coupled plasma optical emission spectrometer (ICP-OES).

Specific Activity Measurements

The enzymatic activity was measured by monitoring oxygen consumption in a Rank Brothers Oxygen Electrode at 37°C as previously reported (22, 38, 42, 44, 45). The reaction was performed in a water-jacketed cell maintained at 37°C. The mixture (2mL) contained 100mM MES pH 5.5, 200μL of 6mg/mL catalase solution (47,000 units/mg), 5μM cupric sulfate solution, 10mM ascorbate and 80μM dansyl-YVG substrate. The reaction mixture was allowed to equilibrate for 1 minute after which it was capped and a baseline was measured for 50s. The reaction was then initiated by adding 10 – 50μL of enzyme (depending on the mutant), through the cap of the reaction vessel with a 50μL Hamilton syringe. The enzyme concentration for mutants was varied from 100μM to 350μM.

X-ray absorption spectroscopy

Oxidized samples were prepared in a single step by 5-fold dilution of 2mM protein in 50mM MES pH 5.5 (4mM in Cu(II)) with the appropriate mixed buffer containing 20% ethylene glycol. Reduced protein samples were prepared under anaerobic conditions by 5-fold dilutions of 2mM protein (4mM in Cu(II)) samples of the oxidized enzyme with the appropriate buffer containing 5mM ascorbate and 20% ethylene glycol. Samples were transferred to an XAS cuvette via a syringe and flash-frozen in liquid nitrogen. Final PHMcc copper concentrations ranged from 600 to 1200 μM.

Copper K-edge (8.9 KeV) extended X-ray absorption fine structure (EXAFS) and X-ray absorption near edge structure (XANES) data were collected at the Stanford Synchrotron

Radiation Lightsource operating at 3 GeV with currents between 300 and 450 mA maintained by continuous top-up. Samples were measured on beamline 7–3 using a Si[220] monochromator and Rh-coated mirror upstream with 13 keV energy cutoff in order to reject harmonics. Data were collected in fluorescence mode using a high-count rate Canberra 30-element Ge array detector with maximum count rates per array element less than 120 kHz. A Z-1 nickel oxide filter and Soller slit assembly inserted in front of the detector was used to reduce elastic scattering relative to the Cu Kα fluorescence. Four to six scans of a sample containing only the buffer were averaged and subtracted from the averaged data for each protein sample to remove the Ni K_β fluorescence and produce a flat pre-edge baseline. Samples were measured as aqueous glasses in 20% ethylene glycol at 10K. Output from each detector channel was inspected for glitches and dropouts before inclusion in the final average. Data reduction and background subtractions were performed using the program modules of EXAFSPAK (46). Spectral simulation was carried out using EXCURVE version 9.2 (47, 48) as described previously (21, 22, 49, 50). Simulations of the EXAFS data used a mixed-shell model consisting of imidazole from histidine and S from methionine coordination. The threshold energy, E0, was chosen at 8985 eV, and refinement of structural parameters included distances (R), coordination numbers (N), and Debye-Waller factors ($2\sigma^2$), and included multiple scattering contributions from outer-shell atoms of imidazole rings.

Stopped-Flow Spectroscopy

The protein sample was left in the anaerobic chamber for 30 minutes to deoxygenate, concentrated in an Amicon filter (10,000 MWCO), and then diluted with argon-purged MES buffer (50mM, pH 5.5) to a final concentration of 50μM. For experiments performed in the presence of substrate, aliquots of stock solutions of Ac-YVG (Km=7 μM), hippuric acid (Km= 1.2 mM) or nitrohippuric acid (Km=470 μM) were added to a final concentration of 100 μM, or in the case of the lower affinity hippuric acid and nitrohippuric acid, 12 mM and 4 mM respectively.

Pre-weighted DMPD salt, syringes, argon-purged deionized water and buffer were made anaerobic by overnight storage in the anaerobic chamber. The 50mM DMPD stock solution was made by dissolving pre-weighed salt in 1ml of deionized water. This DMPD stock solution was used to prepare DMPD solution of 2mM concentration, using deoxygenated deionized water.

Stopped-flow experiments were conducted under anaerobic conditions at room temperature on a SX20 Applied Photophysics stopped-flow instrument enclosed in a Vacuum Atmospheres anaerobic chamber with oxygen levels of 1 ppm.

Analysis of stopped-flow data

DMPD (N, N-dimethyl-1, 4-phenylene diamine) is able to replace the physiological reductant ascorbate, undergoing one-electron oxidation to the radical cation with concomitant reduction of the enzyme copper centers (51). The DMPD radical is a chromophoric agent which absorbs strongly at 515nm (A_{515}) and 550nm (A_{550}) with molar absorptivity at 515nm of 5200M^{-1}cm^{-1}. The formation of the DMPD radical strongly

correlates with the reduction of the copper centers making possible the measurement of copper reduction rates by monitoring the variation of absorbance at 515nm (A_{515}) versus time.

The concentration of the reduced copper was determined from the equation

$$Concentration\ of\ the\ reduced\ copper = \frac{\Delta A_{515}}{\epsilon_{DMPD}} \quad (1)$$

Where A_{515} is the difference in absorption at 515nm at time t, and $\epsilon_{DMPD} = 5200$ $M^{-1}cm^{-1}$. The ratio of reduced copper to protein concentration was calculated for every time point and plotted against the time using SigmaPlot 12.0. The total copper to protein ratio in each sample was also plotted as a reference value. The data were fit to a double exponential equation for samples with both H- and M-sites intact viz (WT PHM, H108A, H172A, and H107A)

$$A_t = A_0 + A_1\left(1 - e^{-k_1 t}\right) + A_2\left(1 - e^{-k_2 t}\right) + ct \quad (2)$$

Where A_1 and A_2 are the absorbance as a function of time for each of the two exponential time courses, putatively corresponding to reduction of the two copper centers with rate constants k_1, k_2 respectively. A_0 is the initial absorbance at time zero. In all experiments it was found that DMPD oxidation continued in a slow, almost linear phase for some time after the absorbance change indicated complete reduction of the copper centers. One explanation for the continued slow DMPD oxidation is enzyme turnover due to traces of oxygen that were not completely scavenged or enzyme instability resulting in other reductive events such as disulfide reduction, but other undefined enzymatic or non-enzymatic processes may also be occurring. To account for this effect, a linear factor (ct) was added to improve the fits at longer times in the reaction.

The reduction data of the mutants having only one of the two sites intact (H107H108A and H242A) were fit to a single exponential equation.

$$A_t = A_0 + A_1\left(1 - e^{-kt}\right) + ct \quad (3)$$

A_1 is the absorbance associated with H-site (H242A) or M-site (H107H108A), A_0 is the initial absorbance at t= 0 and k is the rate constant. As before, a linear factor (ct) was found to improve the fits at long time points, presumably arising from non-catalytic sources of DMPD oxidation.

Protein Film Voltammetery

Protein film voltammetry was used to measure redox potential values of the proteins. A 3–5 ul drop of protein solution was placed on a pyrolytic graphite electrode (PGE) surface and samples were measured either after 3 min or when the drop was dried. All the experiments were performed in degassed 50 mM MES, pH= 6.0 + 100 mM NaCl, on ice, and under Ar flow. The scan rate was either 250 mV/s or 100 mV/s, with a quit time of 2s. Data analysis

was carried out using OriginPro9.0 software (Origin Lab), licensed to University of Illinois at Urbana-Champaign, using the previously reported procedure (52). In brief, the presence of the peaks was confirmed by plotting the first derivative of the initial scans. The raw data was analyzed using the "peak analysis" option in Origin software. Through the process the faradaic capacitance of background was subtracted to obtain the red curves shown in Figure 7 and Figs S5 – 8 of the Supporting Information.

Results

Reduction kinetics of WT PHM

Determining the independent rates of reduction of the H- and M-sites required the enzyme to be stabilized in its fully reduced Cu(I) state. Therefore, to preclude turnover and prevent oxidation of the protein sample, the entire experiment including the sample preparation were done under anaerobic conditions. Figure 2 (top left) shows a representative absorbance versus time plot for DMPD as reductant with associated time course at 515nm as an inset. It can be seen that the absorbance rises rapidly from near zero in the visible (reduced DMPD is colorless) and eventually reaches a constant value. This endpoint represents less than eight percent of the total DMPD present indicating that another species (i.e. the concentration of the enzyme-bound copper) is the limiting reagent. The structure of the Cu(I) centers has previously been studied in detail by XAS for the ascorbate-reduced forms (14, 16, 22) including single site H and M structures (44, 53, 54), reactions with exogenous ligands (38, 55), changes induced by pH (42, 49), and active site mutants (14, 42, 49, 56). To verify that DMPD reduction generated the same reduced enzyme species we first measured the EXAFS spectrum of a DMPD-reduced form of the WT enzyme, and analyzed its metrical parameters in MES buffer at pH 5.5. The results (Fig 2, top right) showed insignificant differences between ligation, bond-lengths and Debye Waller factors of the DMPD and ascorbate-reduced forms. The DMPD-reduced form was simulated by an average per copper coordination of 2.5 histidine and 0.5 S(Met) ligands with bond lengths of 1.96 ± 0.02 Å and 2.27 ± 0.02 Å respectively. This compares favorably with the coordination previously determined for the ascorbate-reduced enzyme at pH 5.5 of 2.5 Cu-His at 1.96 ± 0.02 Å and 2.25 ± 0.02 Å Cu-S(Met) (49). We also investigated the effect of substrate binding to the reduced (Fig. 2, bottom left) and oxidized (Fig. 2, bottom right) enzyme on the EXAFS spectra. These data also confirmed the previous observation that substrate binding induces no structural rearrangement at the copper centers that can be detected within the resolution of the experiment, since the EXAFS data are superimposable.

Figure 3 shows kinetic traces for reduction of WT PHM in absence and presence of the substrate Ac-YVG (open blue circles and open green circles respectively). The dashed line represents the initial total copper to protein ratio at the beginning of the experiment (2.3 Cu per protein). The solid curves represent the simulated traces using fits generated from equation 1. The data show that in the absence of the substrate, approximately half of the total oxidized copper present in the sample is reduced within 200ms followed by the slower reduction of the rest of the oxidized copper present in the sample in a second phase taking ~2.5s to reach completion.

Curve fitting shows that the reduction is a biphasic process with one of the copper centers being reduced in an initial fast phase, followed by a much slower reduction of the other copper center. This is not an entirely unanticipated result since the ligand sets of the copper centers as well as their functions differ. However, at this point it is not possible to assign either rate to a specific Cu center (H or M). The rates of reduction in the presence of the substrate Ac-YVG exhibit different behavior. Although both rates are accelerated, there is a much larger increase in the rate of the slow phase.

The kinetic traces were fit to a double exponential equation to obtain the value of the rate constants which are listed in Table 1. The rate constant of the slow phase (0.46 s^{-1}) is accelerated by a factor of 10 in presence of the substrate (4.2 s^{-1}), whereas the rate constant of the fast phase (17.2 s^{-1}) is accelerated by a factor of 2 (30.8 s^{-1}). Use of the substrate nitrohippuric acid showed a similar trend with the slow and fast rates increasing by factors of 6 and 2 respectively. However, hippuric acid only accelerated the slow phase by 4.3 times and decreased the fast phase by a factor of 1.7 (Table 1 and Figs S1 and S2).

Assigning slow and fast rates to their respective copper centers

In previous work we reported two PHM variants H242A and H107H108A in which one histidine residue at the M center (H242) and two histidine residues at the H center (H107 and H108) were mutated to alanine, and showed that these variants displayed properties consistent with single copper site occupancy at the H and M sites respectively (44). Specifically, ICPOES analysis indicated that each variant bound only a single copper atom, and EXAFS of the reduced forms could be simulated using the expected ligands sets for the chemically inequivalent H (3 His) and M (2His + 1 Met) copper centers respectively. These single site variants were used to assign the fast and slow rates of reduction observed in the WT enzyme to the H and M copper centers. After protein isolation and copper reconstitution, ICPOES was used to confirm copper-to-protein ratios for H242A (H-site) of 0.96, and H107AH108A (M-site) of 0.90, indicating almost full occupancy of the individual centers. Both the mutants were found to be inactive in the assay conducted on the oxygen electrode (data not shown).

Figure 4 (top panel) shows the reduction kinetics of the H242A H-site mutant in presence and absence of Ac-YVG (open blue circles and open green circles respectively). The reduction event is fast and is complete within 150 milliseconds. There is a complete absence of the slow phase. The data fit well to a single exponential equation, further confirming that the reduction is a monophasic event. A higher percentage of copper atoms (92%) was reduced in the presence of the substrate compared to 82% in its absence.

Figure 4 (bottom panel) shows the reduction kinetics of the H107AH108A M-site only mutant in the presence and absence of the substrate Ac-YVG (filled cyan circles and filled purple circles respectively). The time taken for reduction of the single M-site suggests that it is a much slower process. Only 53.4% of the copper in the M-site was reduced by 100 seconds compared to almost complete reduction of H in 150ms. Reduction of the isolated M-center in H107AH108A takes more than 200 seconds to reach completion (data not shown). The presence or absence of substrate has negligible effect on the rate of the

reduction event (Table 2). These results allow us to assign unambiguously the fast reduction rate to the H-site and the slow rate to the M-site in the WT PHM.

Importance of H-site ligand H108 in the ET Process

In an effort to understand the role of H-site ligands in the ET process, reduction kinetics were measured for alanine variants of each of the three H-site ligands (H107A, H108A and H172A). H107A did not show any significant changes in the rate of reduction from the WT PHM (Fig. S3) and was not studied in detail. More interesting results were obtained from the H108A and the H172A mutants. Figure 5 (top panel) shows the reduction kinetics of the H108A mutant in the presence and absence of the substrate Ac-YVG (brown open circles and green open squares respectively) compared with the WT PHM in presence of the substrate Ac-YVG (violet open circles) over a 10 s time interval while Figure 5 (bottom panel) shows the initial 200ms of reaction. The copper to protein ratio for the H108A sample was 1.9, indicating 95% occupancy of both the copper sites. The data highlight two important observations: 1) the slow phase, associated with the M-site is completely absent, and 2) despite the presence of both the copper sites, only half the copper present in the sample is reduced. Since only the fast phase is present it can be concluded that only the H-site is being reduced in the H108A mutant. The data fit well to a single exponential equation (Fig. 5 bottom panel) and the value of the rate constants confirms that the rate of reduction is both fast and monophasic (Table 1). The results show that the M-site is not reduced in the H108A mutant in the time-frame of the experiment (10 s). This very surprising result provides evidence that the electrons are transferred from the H-site to the M-site via a specific path, which is destroyed when H108 is mutated, and imply that H108 is one of the key components of the pathway utilized for delivery of electrons into the M-site.

H172A Reduction Kinetics—We have reported on the structural and kinetic properties of the H172A variant in previous studies. (41, 56) H172A is less than 0.3% active compared to the WT PHM. Copper binding and K_m (Ac-YVG) are not affected but the K_{cat}/K_m (O_2) shows a 300 fold decrease in magnitude compared to the WT enzyme and kinetic isotope analysis suggests a large decrease in the rate of the chemical step (H atom abstraction) (41, 56). Reduction kinetics were performed in the hope of clarifying the role of H172 in the ET process. The total copper to protein ratio in the sample was 1.9, indicating 95% occupancy of both the H- and M-sites. The data for H172A reduction (Figure 6) is similar to that of the WT PHM, with the same characteristics, that is, the reduction is biphasic with a faster phase (<200 milliseconds) and a slow phase (~2.5 seconds). The non-linear regression analysis shows that the rate constant of the fast phase is comparable to that of the WT PHM in the absence of the substrate (Table 1). The slow phase, however, is at least 2.6 times faster and is little changed in the presence of substrate. The results suggest that H172 is not an important pathway residue for electron delivery to the M-center, although the lack of a substrate dependence of the slow rate is puzzling. It is possible that redox potential effects are more important than pathway residues in this variant.

Protein Film Voltammetry—To explore the contribution of changes in redox potential to the reduction rates, we measured the redox potentials of the two copper centers using protein film voltammetry (57–59) For all experiments reversible waves were obtained (Figure 7 and

Figs. S5 – S7). As expected on the basis of the chemical inequivalence of H and M centers, the WT protein generated two waves centered at −15mV and +270mV vs NHE where the more negative value would be consistent with slower M-site reduction and the larger (more positive) value would be consistent with the faster H site reduction. In the presence of the substrate Ac-YVG a single (unresolved) PFV wave was obtained centered at a potential of +83 mV, consistent with the observation that substrate binding decreases the difference in reduction rates of the two copper centers. Experiments using the single H-site variant H242A gave a potential of +213 mV closer to that observed for the WT peak 2 (Table 2). This observation confirms that the fast reduction rate is associated with the H-center. The single M-site variant H107AH108A gave a potential of +140 mV, 60 mV more positive than the WT in the presence of substrate. These data suggest that the M-site potential is very sensitive to changes in its environment induced by nearby substrate binding, as well as more distant effects such as loss of metal from the H-center. Factors such as solvent ordering and/or charge distribution in the active site cleft may also contribute to the observed trends in the redox potentials.

Despite the loss of a coordinating His residue, the H108A and H172A variants each bind 2 coppers (42), and therefore like WT, might be expected to exhibit two separate potentials. However, the H108A variant showed only a single peak with potential of around 270 ±1 mV vs NHE. Since this peak is identical to that observed for WT peak 2 (Table 2) this peak can be assigned to the H-site. Of great interest, the removal of a His ligand to give a 2-coordinate structure as determined from EXAFS studies of this mutant (42) does not appear to perturb the potential in the absence of substrate, giving support to previous conclusions that only two of the three His residues are coordinated in the WT H-center (22, 44). The lack of a peak at lower potentials corresponding to the CuM site may suggest that its observation is limited by slow reduction kinetics which would be in good agreement with our kinetic data where reduction of the CuM site does not occur on the 10 s time scale of the experiment. For H172A we observed a broad peak at around 210 mV vs. NHE, close to that of H108A, and believe that this peak, at least partly, is from the CuH site. The oxidative peak was very small and any effort to increase the signal by increasing the protein concentration or longer incubation times resulted in unfolding the protein and appearance of an intense peak due to unfolded protein (data not shown). Moreover, since the peak was broad, it is possible that it is from two sites, similar to what observed in WT-PHM with peptide. In this case, the result is consistent with faster reduction rates of H172A. However, the resolution of the data and the low stability of H172A on the electrode surface made it hard to draw any definite conclusions.

Discussion

We have investigated the reduction of fully oxidized PHM to its Cu(I)M – Cu(I)H form using the chromophoric reductant DMPD. For the WT protein, a two-step process is observed suggestive of differing rates of reduction for each of the two copper centers. Measurements on the two single site variants H242A (H-site occupied, M-site empty) and H107AH108A (M-site occupied, H-site empty) (44) have allowed us to assign the fast rate to reduction of the H-site and the slow rate to the reduction of the M-site. Whereas the rates of H-site reduction were largely unchanged between WT and the single-site H variant, the

rate of reduction of the M-center was two orders of magnitude slower when the H-center was absent. This latter observation implies a fundamental difference in reduction mechanism between PHM derivatives containing both centers and those where the H-center lacks its metal, and strongly supports a mechanism in which electrons enter preferentially at a site in the vicinity of H, and are then transferred via an intramolecular pathway to the M-center. In the absence of the H-center, this latter pathway is unavailable and reduction likely reverts to a less efficient outer-sphere interaction between the DMPD and the Cu(II)-ligand environment at the M-center.

The pathway for intramolecular electron transfer in PHM and DBM has generated much debate in the literature but current proposals are still speculative. The copper centers are separated by 11 Å of solvent-filled channel (19, 20, 23), while large changes in first-shell coordination spheres occur at both copper centers as the result of reduction of the oxidized protein to the di-Cu(I) form (22). These structural attributes might be expected to inhibit rapid inter-site ET due to the large reorganizational energies anticipated as the result of ligand and solvent rearrangement (38). The shortest "through-bond" pathway is about 80 Å which in the absence of multiple intervening redox centers (60) is too long for efficient intramolecular ET. These factors have prompted a number of alternative suggestions for the preferred ET pathway by mechanisms which allow short-circuiting of the through bond pathway. Jaron and Blackburn initially proposed the superoxide channeling mechanism in which O_2 reacted first with Cu(I) at the CuH-site, and the superoxide that was formed then migrated across the 11 Å solvent-filled cavity and reacted with CuM(I), to generate an "active CuM-peroxo species. This mechanism where the electron is carried by the superoxide entity, predicted that under conditions or with mutants where the reaction is very slow, the superoxide would "leak" out of the cavity and lead to uncoupling of oxygen consumption from substrate hydroxylation. Subsequent observations that oxygen consumption remained 100% coupled to hydroxylation in H172A (41) and M314H (49) even though the catalytic rate had decreased up to 1000-fold rendered this mechanism untenable. A second proposal suggested by Amzel and coworkers on the basis of crystal structures (3, 19, 20) involved an ET pathway comprised of H108, Q170, a water molecule, and the peptide substrate. However, mutation of the critical substrate-mediated pathway residue Q170 had only limited effects on the steady state kinetics (43). A third suggestion from Klinman and coworkers (27) proposed that the electron could transfer across the intersite cavity, perhaps assisted by Y79 provided the solvent was *ordered*. This latter mechanism has also been tested *in silico* where a pathway composed of a chain of three H-bonded water molecules was calculated to have sufficiently low activation energy for rapid proton-coupled ET provided that the CuM-site acceptor was the Cu-O• (cupryl) species (61). A mechanism involving interdomain motion has also been suggested (39), but deemed unlikely on the grounds that the interdomain distance does not change in any of the crystal structures published to date.

PHM is a monooxygenase which means that that the external reductant supplies two of the four electrons necessary to reduce dioxygen, with the other two coming from the activated C-H bond of the substrate. These electrons are stored on the enzyme in the two uncoupled Cu(I) sites but it is important to recognize that they are different mechanistically and are transferred to the catalytic M center at different stages of the reaction cycle. The first

electron reduces the Cu(II)M species to the Cu(I)M state prior to binding of dioxygen at M. The second electron is transferred after the enzyme has committed to catalysis, and is generally believed to reduce a high-valent species such as Cu(III)=O or Cu(II)-O• formed after the O-O bond has broken (26, 61, 62). The present study focuses on the initial reduction of the M-center and therefore relates only to the first electron. To gain further insight, we examined the effect of the presence of peptide substrate on the reduction kinetics.

Binding of Ac-YVG was found to accelerate the rate of M-site reduction in the WT protein by a factor of ~10 (see Table 1), such that the reduction rates of each metal center were less disparate. This result suggests that one important mechanistic attribute of substrate binding is to couple the redox chemistry of the two centers such that they behave more as a coupled system even though they are separated by 11 Å. This electronic coupling could arise from effects on the redox potentials of CuH and CuM (thermodynamic) or from more efficient long-range electronic coupling (kinetic). Data from protein film voltammetry supports an effect on the redox potential as one factor in the substrate activation. Voltammagrams of the WT protein in the absence of substrate show two reversible waves centered at mid-point potentials of +270 mV and −15 mV, while H-site and M-site single site variants show mid-point potentials of 213 and 140 mV respectively. This suggests that E_{red} (WT) = 270 mV can be assigned to the H-center while E_{red} (WT) = −15 mV should be assigned to the M-center. In the presence of substrate only a single reversible wave was observed at E_{red} (WT, Ac-YVG) = 83 mV. The single wave in the presence of substrate could arise from substrate coupling of the two copper centers so that they reduce at the same potential, or to the average of two non-resolvable mid-point potentials of near equivalent value. In either case, the CV data is in good agreement with the kinetic data, and implies that the substrate activates the first reductive step by equalizing the redox potential of each center. Similar substrate activation has been observed in cytochrome P450, where binding of camphor leads to an increase in E_{red} for NADH reduction (63, 64).

The structural origin of substrate redox coupling in the PHM system is of great interest. An increase in M-site potential could be due either to stabilization of the Cu(I)M state or a decrease in the stability of Cu(II)M. In previous work (44) we have established that the thioether ligand of M314 adopts both Met-on and Met-off conformations, since the shell occupancy is substoichiometric, and pH dependent. This suggests that an increase in the occupancy of Met-on conformer might be responsible for the increase in potential, since thioether ligands favor the Cu(I) state. However, a careful comparison of the EXAFS of the reduced protein at pH 5.5 in the presence and absence of YVG failed to detect any change in the intensity of the Cu-S wave. An alternative possibility is that the binding of Ac-YVG to the PHM active site cavity via its salt bridge to R240 neutralizes one positive charge, and affects the electrostatics of the active site cleft. However, this too is problematic, since the effect is in the wrong direction, where decreased positive charge should stabilize the cupric state and/or destabilize the cuprous (65). It is further possible that substrate binding could alter solvent structure and H-bonding interaction in the vicinity of metal centers. Indeed a closer look at the structure of reduced PHM without substrate (PDB ID: 3PHM) and in the presence of substrate (IYG) (PDB ID: 1OPM) showed the possibility of such changes. First and foremost, presence of the substrate would place the M-site in a more hydrophobic

environment. Multiple studies have demonstrated increased hydrophobicity as a contributor to increased reduction potential of a metal site. Aside from this obvious change, subtle changes in the Cu sites can also be detected. As shown in Figure S8, substrate binding causes an overall rearrangement of the solvent structure around the M site. The change in the arrangement of solvent molecules around a metal center has been postulated as a major factor in perturbing the redox potential of the site when other factors remain the same. The H-site also undergoes small but potentially significant geometrical rearrangement of the ligand orientation. Taken together these factors may be sufficient to induce the changes in redox potential that are observed.

To further explore the importance of intersite electronic coupling we examined the reduction rates of H-center variants in which one of the coordinated histidine ligands was mutated to alanine. Previous studies have shown that H-site single histidine to alanine variants (H107A, H108A, H172A) are fully competent to bind Cu(I) in a 2-coordinate structure involving the remaining two His ligands (42). The reduction rates of these variants therefore inform as to which His residue is important in the intramolecular ET pathway. To our surprise we found that whereas H108A could be rapidly reduced by one equivalent per copper, further reduction was not observed on the time scale of the experiment (0 – 10 seconds). We ascribe the first reducing equivalent to the reduction of the H-center which proceeds at a rate comparable to that of the WT protein. The abrogation of any further redox chemistry in this mutant strongly suggests that H108 is an essential element of the exit pathway for the H to M electron transfer. In support of this interpretation, we also observed that in the presence of substrate, the H172A variant was unperturbed relative to the WT protein. Redox potential measurements were also consistent with these arguments, showing only a single wave at 270 mV (Table 2) assignable to the H-center suggesting that redox chemistry at the M-center might be kinetically limiting. (The more positive potential relative to the WT protein is expected on the basis of our recent EXAFS studies which show a 2-coordinate geometry more favorable to Cu(I) (42)). These observations are in good agreement with Amzel's proposed "substrate-mediated" pathway involving H108, Q170, a water molecule, and the peptide substrate. The substrate-induced acceleration of reduction in the WT protein further supports this pathway, where long-distance electronic coupling through the substrate backbone could combine with its effect on redox potential to increase ET rates. The fast rates exhibited by the H172A variant in the *absence* of substrate are puzzling, and are not fully accommodated by the model, but it is possible that this mutation alters the intersite structure such that the advantage of electronic coupling via the substrate is lost.

While substrate mediated ET is an attractive hypothesis, and appears to be consistent with our new data, the failure of a Q170A mutation to abrogate catalysis has cast doubt on its validity (43). The alternative pathway via His172 and the nearby Y79 which π-stacks against the histidine ring has been evaluated both experimentally (27, 41) and computationally (61). In this pathway, the tyrosine is about 7 Å from the CuM center, and could operate as a facile ET pathway provided the intervening solvent is ordered. To evaluate the importance of this pathway, PHM H172A, and TBM Y216W, I and A variants have been studied. Detailed kinetic analysis of PHM H172A (41) based on both steady state and kinetic isotope data reported a 3 order-of-magnitude decrease in k_{cat}. Since this mutant bound copper with ratios close to that of the WT enzyme (56), the effect was not due to loss of copper from the H-

center. Rather, and consistent with other His to Ala variants at the H center (42), the CuH structure was proposed to be 2-coordinate, retaining its H107, and H108 ligands (56). The impaired activity was traced to a dramatic reduction in the rate of C-H bond cleavage in the chemical step of the mechanism which was suggested to arise from perturbation of important H-bonding networks that modulate H-atom tunneling during the HAT chemistry. Thus, while the mutation of H172 was expected to impact H-site redox potentials and exit pathways, any decrease in ET rate was masked by the larger decrease in the rate of H-atom abstraction. For TBM Y216 variants (PHM Y79 homologues) a comparable effect on the HAT step was not observed, allowing the ET rates to be estimated. Here, the alanine mutation resulted in a profound decrease in H to M ET rate, such that it was now rate limiting. This work provided compelling evidence that a pathway that includes the Y79 residue must be important at least during the irreversible steps following dioxygen binding and activation.

We are therefore presented with two seemingly inconsistent findings (i) the H108 – water – substrate pathway is implicated from the present work, and (ii) that the H172 – Y79 – water pathway is implicated from previous work. However, these results are not necessarily inconsistent if we recognize that (as discussed above) the two electrons stored on the enzyme are different mechanistically and are transferred to the catalytic M center at different stages of the reaction cycle. The first electron reduces the Cu(II)M species to the Cu(I)M state prior to binding of dioxygen at CuM (the reductive electron) while the second electron is transferred after the enzyme has committed to catalysis (the catalytic electron). The pathway for each of these electrons need not be the same, and here we propose a new hypothesis that indeed they are not the same. We propose that H108 and a substrate molecule are involved in the *reductive* pathway while H172 and Y79 are important in the *catalytic* pathway. This hypothesis then allows us to rationalize an additional unique property of this class of monooxygenases, that substrate hydroxylation remains fully coupled to oxygen reduction even with very slow substrates (26), and with mutants of very low specific activity (41, 42). Our hypothesis posits that electron transfer is *gated* such that the catalytic electron can only flow from CuH to CuM after the enzyme has committed to catalysis. Otherwise with slow substrates or mutants, reduction of the Cu(II)-superoxo to peroxide could not be prevented, leading to uncoupling. By utilizing bifurcated ET, the enzyme can "gate" each pathway so that it is only operative during the appropriate phase of the reaction.

The means by which the enzyme might gate these two ET pathways are unknown, but our work suggests a number of possibilities. First, we know from previous EXAFS studies on WT (22) and the H242A H-single site variant (44) that one of the three His residues at CuH is very weakly bound; second, XAS on all three His to Ala variants at the H-site have established that the site becomes stably occupied by Cu(I) provided any two His ligands are present (42); and third removal of a His ligand at the H-center (H108A) does not perturb the E_m value in the absence of bound substrate. From these observations we predict that stable enzyme states can exist with H108 and H172 in either coordinated (on-states) or dissociated (off-states). This implies that H108 can act as a gate for transfer via the H108 –Q170-water-substrate pathway while H172 can act as a gate for the H172-Y79-water pathway. The gate is open when the ligand is "on" and closed when it is "off". The finding from the present

study that H108A abrogates H to M transfer fully supports this idea. We can then model the ensuing gated chemistry as follows. The cycle begins with the oxidized enzyme having both coppers in the Cu(II) state, and CuH coordinated by all three histidines. Electrons enter the H site and can rapidly transfer to CuM via the H108—substrate pathway. A second electron enters the H-site but now the preferred enzyme state is a 2-coordinate H-center with H108 in the off position and H172 in the on position generating the fully reduced di-Cu(I) state ready to bind O_2. Since the gate is closed, no further ET from H to M is possible, and this form of the enzyme is therefore protected from uncoupling reactions that would generate H_2O_2 at the M site. As the catalytic chemistry progresses an enzyme state is reached which is able to turn on the catalytic gate via H172 and Y79. It has been proposed that this event may be initiated by formation of a high potential intermediate such as a high-valent Cu(III)-oxo or Cu(II)-O •-species which is able to overcome the high reorganizational energy for ET through the H172-Y79 –water pathway (24, 61). One hypothesis worthy of merit posits that the electron "hops" from Y79 to the high-potential intermediate, forming a transient tyrosyl radical hole. This process would require a potential of at least 920 mV (66) which would only be accessible after O-O bond breaking such that formation of the tyrosyl hole would be gated by the catalytic chemistry (67). Electron hopping through tyrosine or tryptophan residues has been well documented in ribonucleotide reductase (60), TTQ cofactor formation in methylamine dehydrogenase catalyzed by MauG (68, 69), and photosynthetic reaction centers (70), and modeled by introducing nitrotyrosinate residues into ET pathways in azurin (71). These studies have emphasized the importance of proton coupled oxidation (PCET) mechanisms for tyrosine hole formation since the phenol moiety must be deprotonated in order for oxidation to proceed at accessible potentials, requiring the presence of a proton acceptor which is usually H-bonded to the phenolate OH. We note that in the PHM system, an ordered chain of H-bonded water molecules bridging the phenolate and cupryl intermediate could fulfil this function, since a proton could be transferred via the H-bond network to the cupryl species as the tyrosyl oxidation proceeded. Further, the requirement for coupled proton transfer would provide additional tuning of the gate, since ET could only progress when the solvent was properly ordered between donor and acceptor. The final electron transfer from CuH to Y• would occur rapidly via the π-stacked H172 residue.

It is important to note that mutagenesis of PHM-Y79 to W reduced V_{max} 200 fold (43), while the effect of mutation of TBM-Y216 to W or I was minor, and could be traced primarily to changes in the rates of substrate and product release (27). Whereas tryptophan radical holes have been implicated in MauG (69), the insensitivity of the TBM catalysis to isoleucine substitution suggests that aromatic radical hole formation is not an essential factor. An alternative hypothesis for the ET pathway of the catalytic electron has recently been suggested from studies on the TBM system. Unlike the TBM Y216W/I variants, the TBM Y216A mutant shows rate-limiting electron transfer (27), which has allowed the deuterium solvent isotope effect on this rate constant to be determined (40). The size of this isotope effect and its T-dependence indicate a large entropic contribution to the driving force, suggesting solvent reorganization as a critical step in the catalytic ET process. The data lead to the conclusion that the phenol moiety of Y216 (PHM Y79) participates in, and

helps to pre-organize a network of ordered water molecules which extend from the H site to the M-site. How the protein might "gate" this solvent organization is an open question.

Supplementary Material

Refer to Web version on PubMed Central for supplementary material.

Acknowledgments

aAbbreviations used

ET	electron transfer
MES	2-(N-morpholino)ethanesulfonic acid
dansyl-YVG	dansyl- Tyr-Val-Gly
PHM	peptidylglycine monooxygenase
EXAFS	extended X-ray absorption fine structure
XAS	X-ray absorption spectroscopy
ICP-OES	inductively coupled plasma- optical emission spectrometry
WT	wild-type
Dhfr	dyhydrofolate reductase gene
CHO	chinese hamster ovary
DMEM F-12	Dulbecco's modified Eagle's medium
FBS FCII	fetal clone II
SDS-PAGE	sodium dodecyl sulfate polyacrylamide gel electrophoresis
PBS	phosphate buffer saline
ECS	extra capillary space
MWCO	molecular weight cut off
DMPD	N, N-dimethyl-p-phenylenediamine dihydrochloride

References

1. Eipper BA, Stoffers DA, Mains RE. The biosynthesis of neuropeptides. Ann Rev Neurosci. 1992; 15:57–85. [PubMed: 1575450]

2. Kulathila R, Merkler KA, Merkler DJ. Enzymatic formation of C-terminal amides. Nat Prod Rep. 1999; 16:145–154. [PubMed: 10331284]

3. Prigge ST, Mains RE, Eipper BA, Amzel LM. New insights into copper monooxygenases and peptide amidation: structure, mechanism and function. Cell Mol Life Sci. 2000; 57:1236–1259. [PubMed: 11028916]

4. Deacon CF. Therapeutic strategies based on glucagon-like peptide 1. Diabetes. 2004; 53:2181–2189. [PubMed: 15331525]

5. Yu JH, Kim MS. Molecular mechanisms of appetite regulation. Diabetes Metab J. 2012; 36:391–398. [PubMed: 23275931]

6. Eipper BA, Milgram SL, Husten EJ, Yun HY, Mains RE. Peptidylglycine alpha-amidating monooxygenase: a multifunctional protein with catalytic, processing, and routing domains. Protein Sci. 1993; 2:489–497. [PubMed: 8518727]

7. Husten EJ, Eipper BA. The membrane-bound bifunctional peptidylglycine a-amidating monooxygenase protein. Exploration of its domain structure through limited proteolysis. J Biol Chem. 1991; 266:17004–17010. [PubMed: 1894599]

8. Bell J, Ash DE, Snyder LM, Kulathila R, Blackburn NJ, Merkler DJ. Structural and functional investigations on the role of zinc in bifunctional rat peptidylglycine a-amidating enzyme. Biochemistry. 1997; 36:16239–16246. [PubMed: 9405058]

9. Chufan EE, De M, Eipper BA, Mains RE, Amzel LM. Amidation of bioactive peptides: the structure of the lyase domain of the amidating enzyme. Structure. 2009; 17:965–973. [PubMed: 19604476]

10. Bradbury AF, Smyth DG. Peptide amidation. Trends Biochem Sci. 1991; 16:112–115. [PubMed: 2057999]

11. Katopodis AG, Ping D, May SW. A novel enzyme from bovine neurointermediate pituitary catalyzes dealkylation of a-hydroxyglycine derivatives, thereby functioning sequentially with peptidylglycine a-amidating monooxygenase in peptide amidation. Biochemistry. 1990; 29:6115–6120. [PubMed: 2207061]

12. Young SD, Tamburini PP. Enzymatic peptidyl a-amidation proceeds through formation of an a hydroxyglycine intermediate. J Am Chem Soc. 1989; 111:1933–1934.

13. Klinman JP. The copper-enzyme family of dopamine b -monooxygenase and peptidylglycine a -hydroxylating monooxygenase: Resolving the chemical pathway for substrate hydroxylation. J Biol Chem. 2006; 281:3013–3016. [PubMed: 16301310]

14. Hess CR, Klinman JP, Blackburn NJ. The copper centers of tyramine beta-monooxygenase and its catalytic-site methionine variants: an X-ray absorption study. J Biol Inorg Chem. 2010; 15:1195–1207. [PubMed: 20544364]

15. Hess CR, McGuirl MM, Klinman JP. Mechanism of the insect enzyme, tyramine beta-monooxygenase, reveals differences from the mammalian enzyme, dopamine beta-monooxygenase. J Biol Chem. 2008; 283:3042–3049. [PubMed: 18032384]

16. Boswell JS, Reedy BJ, Kulathila R, Merkler DJ, Blackburn NJ. Structural investigations on the coordination environment of the active-site copper centers of recombinant bifunctional peptidylglycine a-amidating enzyme. Biochemistry. 1996; 35:12241–12250. [PubMed: 8823157]

17. Eipper BA, Quon ASW, Mains RE, Boswell JS, Blackburn NJ. The catalytic core of peptidylglycine a-hydroxylating monooxygenase: investigation by site-directed mutagenesis, Cu x-ray absorption spectroscopy, and electron paramagnetic resonance. Biochemistry. 1995; 34:2857–2865. [PubMed: 7893699]

18. Kolhekar AS, Keutman HT, Mains RE, Quon ASW, Eipper BA. Peptidylglycine a-hydroxylating monooxygenase: active site residues, disulfide linkages, and a two-domain model of the catalytuc core. Biochemistry. 1997; 36:10901–10909. [PubMed: 9283080]

19. Prigge ST, Kolhekar AS, Eipper BA, Mains RE, Amzel LM. Amidation of bioactive peptides: the structure of peptidylglycine a-hydroxylating monooxygenase. Science. 1997; 278:1300–1305. [PubMed: 9360928]

20. Prigge ST, Kolhekar AS, Eipper BA, Mains RE, Amzel LM. Substrate-mediated electron transfer in peptidylglycine a-hydroxylating monooxygenase. Nature Struct Biol. 1999; 6:976–983. [PubMed: 10504734]

21. Blackburn NJ, Hasnain SS, Pettingill TM, Strange RW. Copper K-EXAFS studies of oxidized and reduced dopamine-b-hydroxylase: confirmation of a sulfur ligand to Cu(I) in the reduced enzyme. J Biol Chem. 1991; 266:23120–23127. [PubMed: 1744110]

22. Blackburn NJ, Rhames FC, Ralle M, Jaron S. Major changes in copper coordination accompany reduction of peptidylglycine monooxygenase. J Biol Inorg Chem. 2000; 5:341–353. [PubMed: 10907745]

23. Prigge ST, Eipper BA, Mains RE, Amzel M. Dioxygen binds end-on to mononuclear copper in a precatalytic enzyme complex. Science. 2004; 304:864–867. [PubMed: 15131304]

24. Chen P, Solomon EI. Oxygen activation by the noncoupled binuclear copper site in peptidylglycine a-hydroxylating monooxygenase. Reaction mechanism and role of the noncoupled nature of the active site. J Am Chem Soc. 2004; 126:4991–5000. [PubMed: 15080705]

25. Chen P, Solomon EI. O_2 activation by binuclear Cu sites: noncoupled versus exchange coupled reaction mechanisms. Proc Natl Acad Sci U S A. 2004; 101:13105–13110. [PubMed: 15340147]

26. Evans JP, Ahn K, Klinman JP. Evidence that dioxygen and substrate activation are tightly coupled in dopamine b -monooxygenase: Implications for oxygen activation. J Biol Chem. 2003; 278:49691–49698. [PubMed: 12966104]

27. Osborne RL, Zhu H, Iavarone AT, Blackburn NJ, Klinman JP. Interdomain Long-Range Electron Transfer Becomes Rate-Limiting in the Y216A Variant of Tyramine beta-Monooxygenase. Biochemistry. 2013; 52:1179–1191. [PubMed: 23320946]

28. Freeman JC, Villafranca JJ, Merkler DJ. Redox cycling of enzyme-bound copper during peptide amidation. J Am Chem Soc. 1993; 115:4923–4924.

29. Merkler DJ, Kulathila R, Consalvo AP, Young SD, Ash DE. Oxygen-18 isotopic carbon-13 NMR shift as proof that bifunctional peptidylglycine a-amidating enzyme is a monooxygenase. Biochemistry. 1992; 31:7282–7288. [PubMed: 1387319]

30. Murthy ASN, Keutmann HT, Eipper BA. Further characterization of peptidylglycine. alpha.-amidating monooxygenase from bovine neurointermediate pituitary. Mol Endocrinol. 1987; 1:290–299. [PubMed: 3453894]

31. McIntyre NR, Lowe EW Jr, Belof JL, Ivkovic M, Shafer J, Space B, Merkler DJ. Evidence for substrate preorganization in the peptidylglycine alpha-amidating monooxygenase reaction describing the contribution of ground state structure to hydrogen tunneling. J Am Chem Soc. 2010; 132:16393–16402. [PubMed: 21043511]

32. Francisco WA, Merkler DJ, Blackburn NJ, Klinman JP. Kinetic mechanism and intrinsic isotope effects for the peptidylglycine a-amidating enzyme reaction. Biochemistry. 1998; 37:8244–8252. [PubMed: 9609721]

33. Bauman AT, Yukl ET, Alkevich K, McCormack AL, Blackburn NJ. The hydrogen peroxide reactivity of peptidylglycine monooxygenase supports a Cu(II)-superoxo catalytic intermediate. J Biol Chem. 2006; 281:4190–4198. [PubMed: 16330540]

34. Crespo A, Marti MA, Roitberg AE, Amzel LM, Estrin DA. The catalytic mechanism of peptidylglycine a-hydroxylating monooxygenase investigated by computer simulation. J Am Chem Soc. 2006; 128:12817–12828. [PubMed: 17002377]

35. Abad E, Rommel JB, Kastner J. Reaction mechanism of the bicopper enzyme peptidylglycine alpha-hydroxylating monooxygenase. J Biol Chem. 2014; 289:13726–13738. [PubMed: 24668808]

36. Francisco WA, Knapp MJ, Blackburn NJ, Klinman JP. Hydrogen tunneling in peptidylglycine a-hydroxylating monooxygenase. J Am Chem Soc. 2002; 124:8194– 8195. [PubMed: 12105892]

37. Moser CC, Anderson JL, Dutton PL. Guidelines for tunneling in enzymes. Biochim Biophys Acta. 2010; 1797:1573–1586. [PubMed: 20460101]

38. Jaron S, Blackburn NJ. Does superoxide channel between the copper centers in peptidylglycine monooxygenase? A new mechanism based on carbon monoxide reactivity. Biochemistry. 1999; 38:15086–15096. [PubMed: 10563791]

39. Owen TC, Merkler DJ. A new proposal for the mechanism of glycine hydroxylation as catalyzed by peptidylglycine alpha-hydroxylating monooxygenase (PHM). Med Hypotheses. 2004; 62:392–400. [PubMed: 14975510]

40. Zhu H, Sommerhalter M, Nguy AK, Klinman JP. Solvent and Temperature Probes of the Long-Range Electron-Transfer Step in Tyramine beta-Monooxygenase: Demonstration of a Long-Range Proton-Coupled Electron-Transfer Mechanism. J Am Chem Soc. 2015; 137:5720–5729. [PubMed: 25919134]

41. Evans JP, Blackburn NJ, Klinman JP. The catalytic role of the copper ligand H172 of peptidylglycine a-hydroxylating monooxygenase: a kinetic study of the H172A mutant. Biochemistry. 2006; 45:15419–15429. [PubMed: 17176064]

42. Kline CD, Mayfield M, Blackburn NJ. HHM motif at the CuH-site of peptidylglycine monooxygenase is a pH-dependent conformational switch. Biochemistry. 2013; 52:2586–2596. [PubMed: 23530865]

43. Bell J, El Meskini R, D'Amato D, Mains RE, Eipper BA. Mechanistic investigation of peptidylglycine a-hydroxylating monooxygenase via intrinsic tryptophan fluorescence and mutagenesis. Biochemistry. 2003; 42:7133–7142. [PubMed: 12795609]

44. Chauhan S, Kline CD, Mayfield M, Blackburn NJ. Binding of Copper and Silver to Single-Site Variants of Peptidylglycine Monooxygenase Reveals the Structure and Chemistry of the Individual Metal Centers. Biochemistry. 2014; 53:1069–1080. [PubMed: 24471980]

45. Bauman AT, Ralle M, Blackburn N. Large scale production of the copper enzyme peptidylglycine monooxygenase using an automated bioreactor. Protein Expression and Purification. 2007; 51:34–38. [PubMed: 16931045]

46. George, GN. EXAFSPAK. Stanford Synchrotron Radiation Laboratory; Menlo Park, CA: 1995.

47. Binsted N, Hasnain SS. State of the art analysis of whole X-ray absorption spectra. J Synchrotron Rad. 1996; 3:185–196.

48. Gurman SJ, Binsted N, Ross I. A rapid, exact, curved-wave theory for EXAFS calculations. II The multiple-scattering contributions. J Phys C. 1986; 19:1845–1861.

49. Bauman AT, Broers BA, Kline CD, Blackburn NJ. A Copper-Methionine Interaction Controls the pH-Dependent Activation of Peptidylglycine Monooxygenase. Biochemistry. 2011; 50:10819–10828. [PubMed: 22080626]

50. Strange RW, Blackburn NJ, Knowles PF, Hasnain SS. X-ray absorption spectroscopy of metal-histidine coordination in metalloproteins. Exact simulation of the EXAFS of tetraimidazole-copper(II) nitrate and other copper-imidazole complexes by the use of a multiple scattering treatment. J Am Chem Soc. 1987; 109:7157–7162.

51. Li C, Oldham CD, May SW. NN-dimethyl-1,4-phenylenediamine as an alternative reductant for peptidylglycine a-amidating monooxygenase catalysis. Biochem J. 1994; 300:31–36. [PubMed: 8198547]

52. Hosseinzadeh P, Marshall NM, Chacon KN, Yu Y, Nilges MJ, New SY, Tashkov SA, Blackburn NJ, Lu Y. Design of a single protein that spans the entire 2-V range of physiological redox potentials. Proc Natl Acad Sci USA. 2015

53. Jaron S, Blackburn NJ. Characterization of a half-apo derivative of peptidylglycine monooxygenase. Insight into the reactivity of each active site copper. Biochemistry. 2001; 40:6867–6875. [PubMed: 11389601]

54. Reedy BJ, Blackburn NJ. Preparation and characterization of half-apo dopamine-b-hydroxylase by selective removal of Cu$_A$: Identification of a sulfur ligand at the dioxygen binding site by EXAFS and FTIR. J Am Chem Soc. 1994; 116:1924–1931.

55. Pettingill TM, Strange RW, Blackburn NJ. Carbonmonoxy dopamine-b-hydroxylase: structural characterization by FTIR, fluorescence and XAS spectroscopy. J Biol Chem. 1991; 266:16996–17003. [PubMed: 1894598]

56. Jaron S, Mains RE, Eipper BA, Blackburn NJ. The catalytic role of the copper ligand H172 of peptidylglycine a -hydroxylating monooxygenase (PHM): a spectroscopic study of the H172A mutant. Biochemistry. 2002; 41:13274–13282. [PubMed: 12403629]

57. Armstrong FA. Insights from protein film voltammetry into mechanisms of complex biological electron-transfer reactions. J Chem Soc Dalton Trans. 2002:661–671.

58. Leger C, Elliott SJ, Hoke KR, Jeuken LJ, Jones AK, Armstrong FA. Enzyme electrokinetics: using protein film voltammetry to investigate redox enzymes and their mechanisms. Biochemistry. 2003; 42:8653–8662. [PubMed: 12873124]

59. Marshall NM, Garner DK, Wilson TD, Gao YG, Robinson H, Nilges MJ, Lu Y. Rationally tuning the reduction potential of a single cupredoxin beyond the natural range. Nature. 2009; 462:113–116. [PubMed: 19890331]

60. Minnihan EC, Nocera DG, Stubbe J. Reversible, long-range radical transfer in E. coli class Ia ribonucleotide reductase. Acc Chem Res. 2013; 46:2524–2535. [PubMed: 23730940]

61. Cardenas DJ, Cuerva JM, Alias M, Bunuel E, Campana AG. Water-based hydrogen-atom wires as mediators in long-range proton-coupled electron transfer in enzymes: a new twist on water reactivity. Chemistry. 2011; 17:8318–8323. [PubMed: 21671300]

62. Chen P, Root DE, Campochiaro C, Fujisawa K, Solomon EI. Spectroscopic and electronic structure studies of the diamagnetic side-on CuII-superoxo complex Cu(O2)[HB(3-R-5-iPrpz)3]: antiferromagnetic coupling versus covalent delocalization. J Am Chem Soc. 2003; 125:466–474. [PubMed: 12517160]

63. Denisov IG, Makris TM, Sligar SG, Schlichting I. Structure and chemistry of cytochrome P450. Chem Rev. 2005; 105:2253–2277. [PubMed: 15941214]

64. Sligar SG, Gunsalus IC. A thermodynamic model of regulation: modulation of redox equilibria in camphor monoxygenase. Proc Natl Acad Sci U S A. 1976; 73:1078–1082. [PubMed: 1063390]

65. Yu F, Penner-Hahn JE, Pecoraro VL. De Novo-Designed Metallopeptides with Type 2 Copper Centers: Modulation of Reduction Potentials and Nitrite Reductase Activities. J Am Chem Soc. 2013

66. Berry BW, Martinez-Rivera MC, Tommos C. Reversible voltammograms and a Pourbaix diagram for a protein tyrosine radical. Proc Natl Acad Sci U S A. 2012; 109:9739–9743. [PubMed: 22675121]

67. Warren JJ, Winkler JR, Gray HB. Redox properties of tyrosine and related molecules. FEBS Lett. 2012; 586:596–602. [PubMed: 22210190]

68. Choi M, Shin S, Davidson VL. Characterization of electron tunneling and hole hopping reactions between different forms of MauG and methylamine dehydrogenase within a natural protein complex. Biochemistry. 2012; 51:6942–6949. [PubMed: 22897160]

69. Tarboush NA, Jensen LM, Yukl ET, Geng J, Liu A, Wilmot CM, Davidson VL. Mutagenesis of tryptophan199 suggests that hopping is required for MauG-dependent tryptophan tryptophylquinone biosynthesis. Proc Natl Acad Sci USA. 2011; 108:16956–16961. [PubMed: 21969534]

70. Barry BA. Proton coupled electron transfer and redox active tyrosines in Photosystem II. J Photochem Photobiol B. 2011; 104:60–71. [PubMed: 21419640]

71. Warren JJ, Herrera N, Hill MG, Winkler JR, Gray HB. Electron flow through nitrotyrosinate in Pseudomonas aeruginosa azurin. J Am Chem Soc. 2013; 135:11151–11158. [PubMed: 23859602]
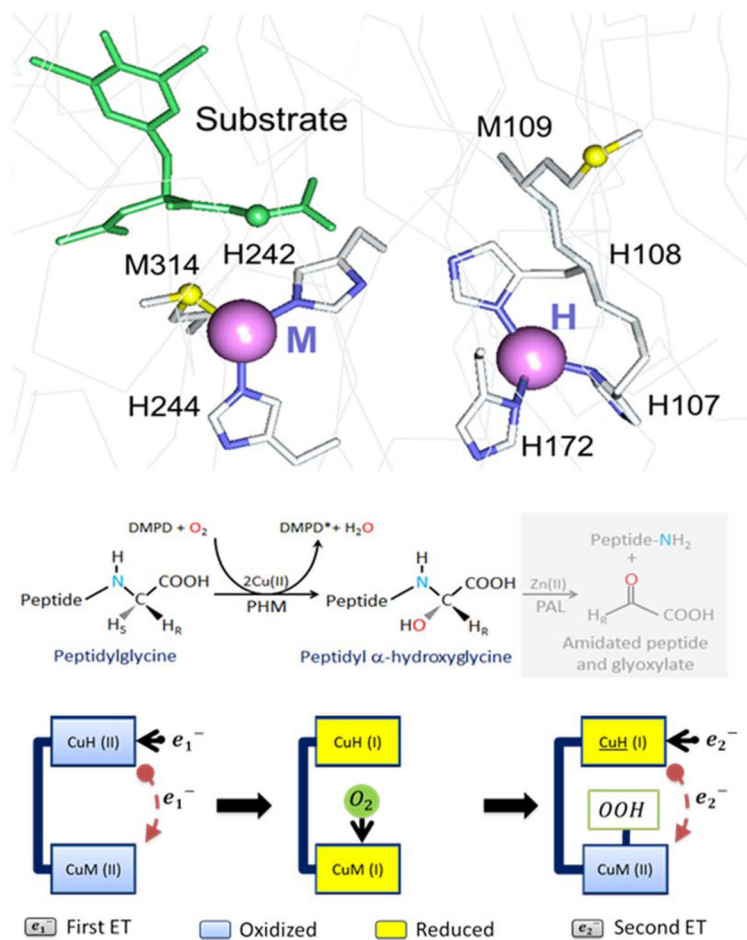
Figure 1.
Top: Active site structure of PHM showing the M-center (left) and H-center (right) with substrate shown in green, binding close to M. Taken from PDB file 1OPM. Middle: Reaction catalyzed by PAM, showing the PHM-catalyzed hydroxylation of the C-terminal Gly residue in bold, and the PAL-catalyzed N-dealkylation shaded. Bottom: Reductive and oxidative (catalytic) phases of the reaction cycle.
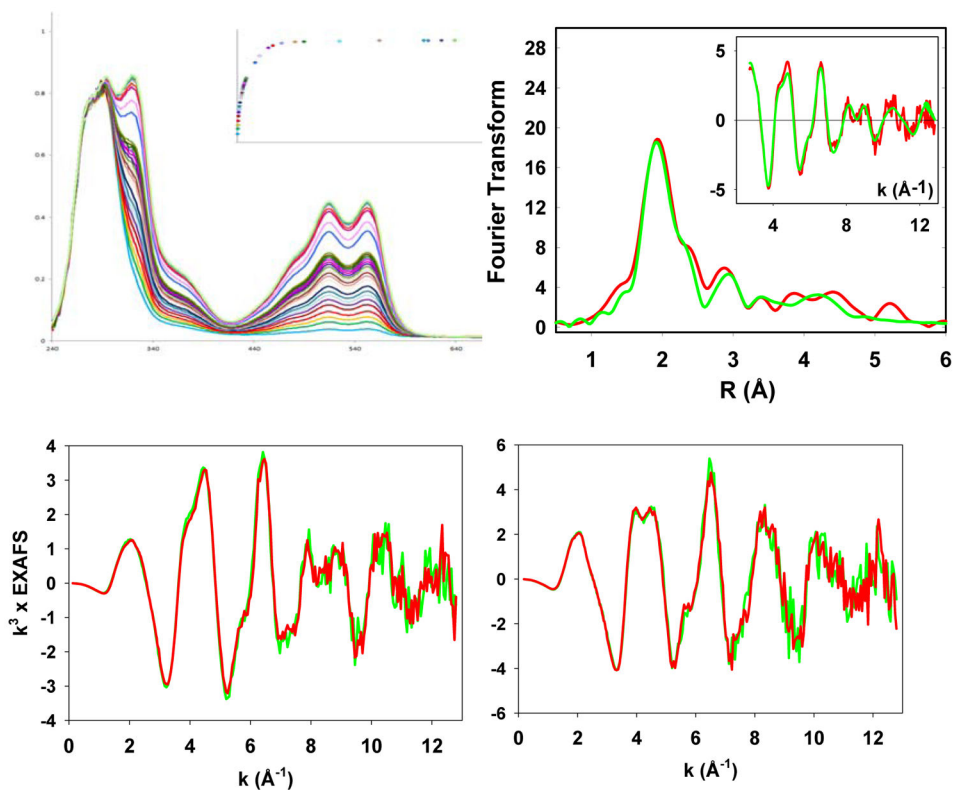
Figure 2.
Spectroscopic features of PHM reduction by DMPD. (Top left) Stopped-flow absorbance versus time plot showing increasing absorbance in the visible due to formation of the DMPD cation radical one-electron oxidized species. (Top right) Fourier transforms and EXAFS (inset) for the DMPD-reduced PHM Cu(I) centers: experimental data are in red, simulated data in green. EXAFS data are shifted in k-space by an amount corresponding to the theoretical energy threshold. Parameters used in this fit are given in Table S1 of the SI. Bottom panels: Comparisons of DMPD-reduced (left) and oxidized (right) PHM in the absence (red) and presence (green) of the substrate Av-YVG.
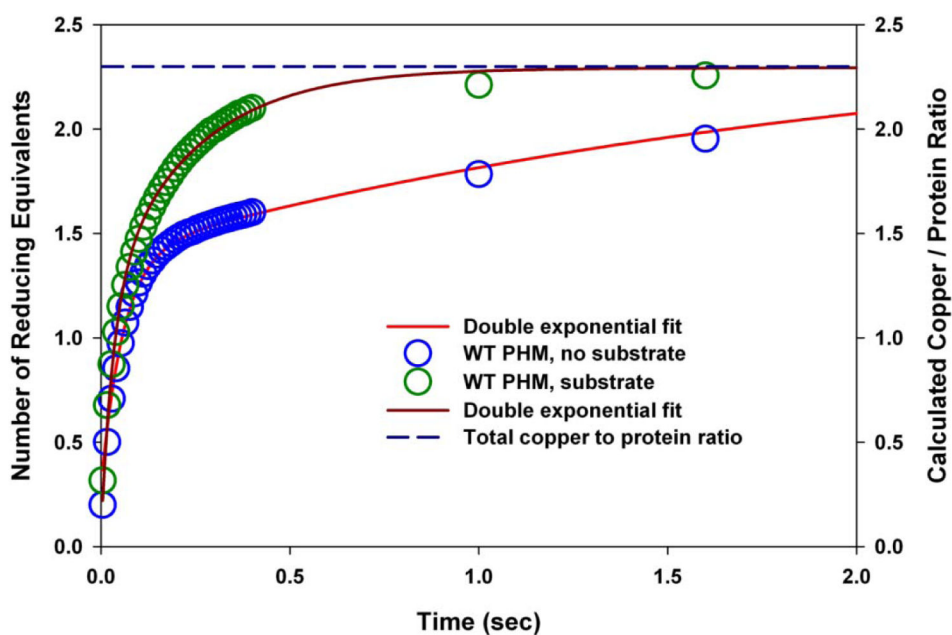
Figure 3.
Reduction kinetics of the WT PHM (0–2 seconds). Open blue circles: WT PHM in the absence of substrate along with the double exponential fit (red line); open green circles: WT PHM in presence of the substrate Ac-YVG along with the double exponential fit (brown line) The dashed blue line represents the total copper to protein ratio in the WT PHM sample. The parameters used for the fits are listed in Table 1. Note: The split time-base used to capture the end point of the slower phase results in fewer time points after 400 ms..
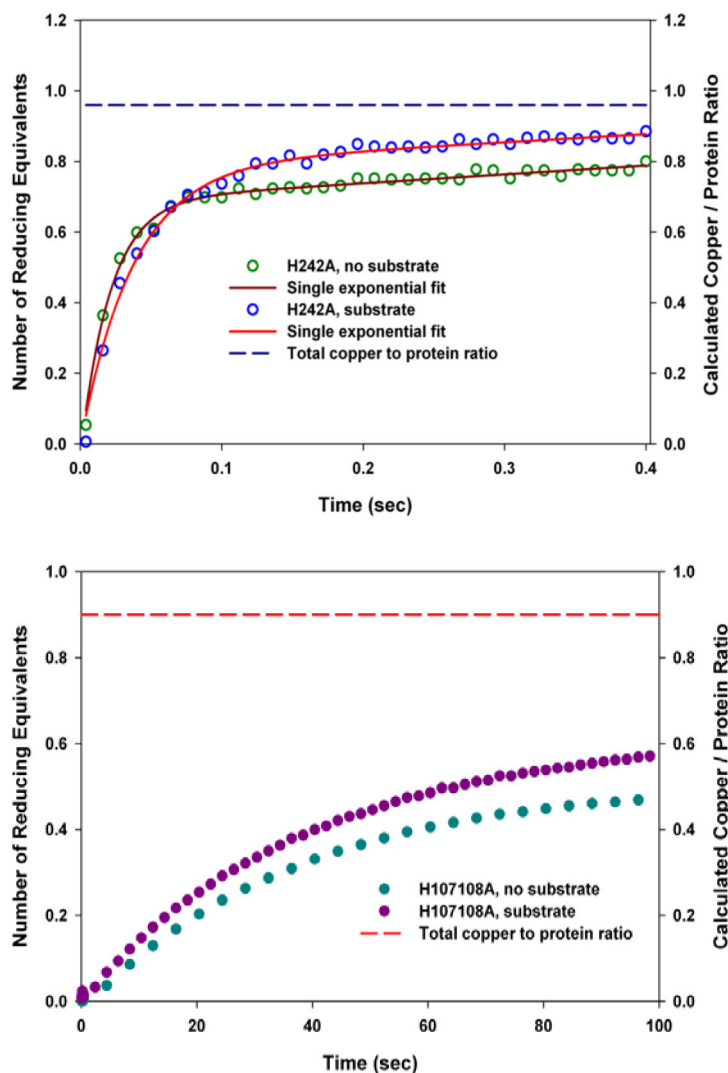
Figure 4.
Top: Stopped-flow reduction kinetic traces of the H242A mutant (H-site only) (0–400ms) in the absence of substrate (open green circles) fitted to a single exponential (brown line) and in presence of the substrate Ac-YVG (open blue circles) fitted to a single exponential (red line). The dashed blue line represents the total copper to protein ratio in the H242A sample. Bottom: Stopped-flow reduction kinetic traces of the H107H108A mutant (M-site only) (0–100 seconds) in the absence of substrate (filled cyan circles) and in presence of the substrate Ac-YVG (filled purple circles) The dashed red line represents the total copper to protein ratio in the H107108A sample. The parameters used for the fits are listed in Table 1.
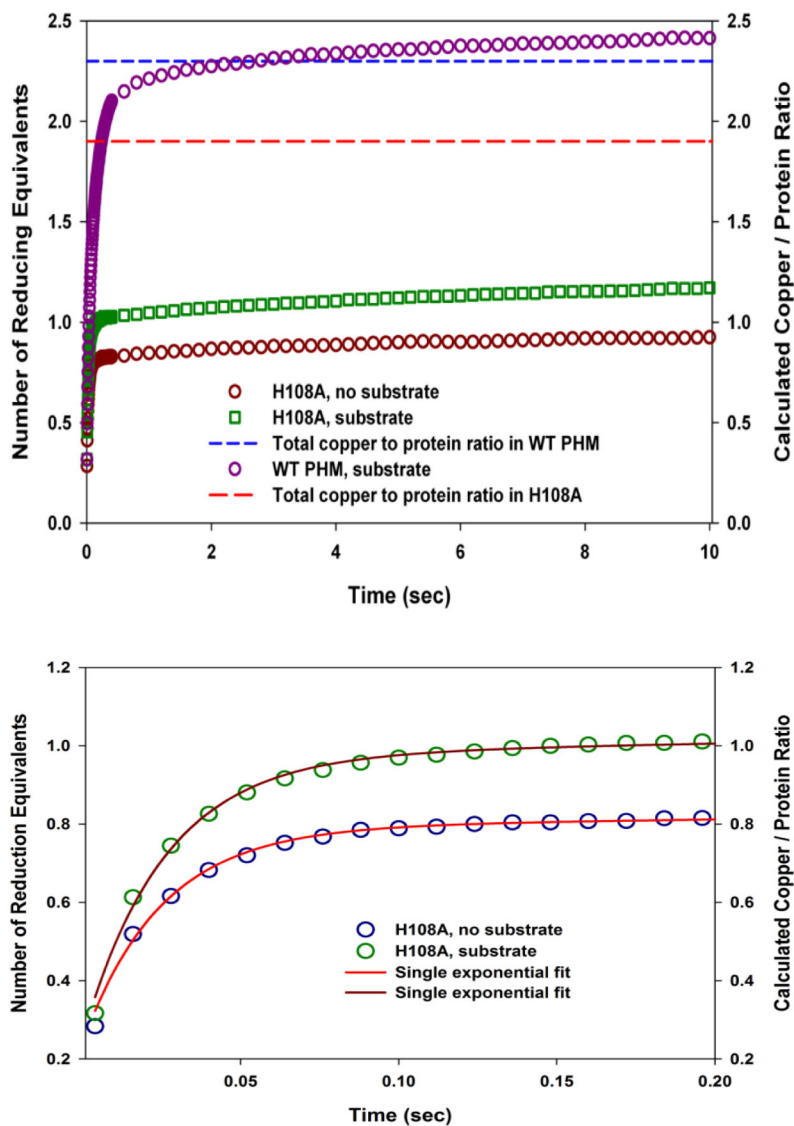
Figure 5.
Top: Stopped-flow reduction kinetic traces of the H108A mutant (0–10 seconds in the absence of substrate Ac-YVG (open brown circles) and in presence of the substrate Ac-YVG (open green squares). Data for WT PHM in the presence of substrate Ac-YVG is shown for comparison (open purple circles). The red and the blue dashed lines represent total copper to protein ratio in the H108A and the WT PHM samples respectively. Bottom: Expanded view of the first 0–200 ms of data for the H108A variant fitted to single exponential fits. The parameters used for the fits are listed in Table 1.
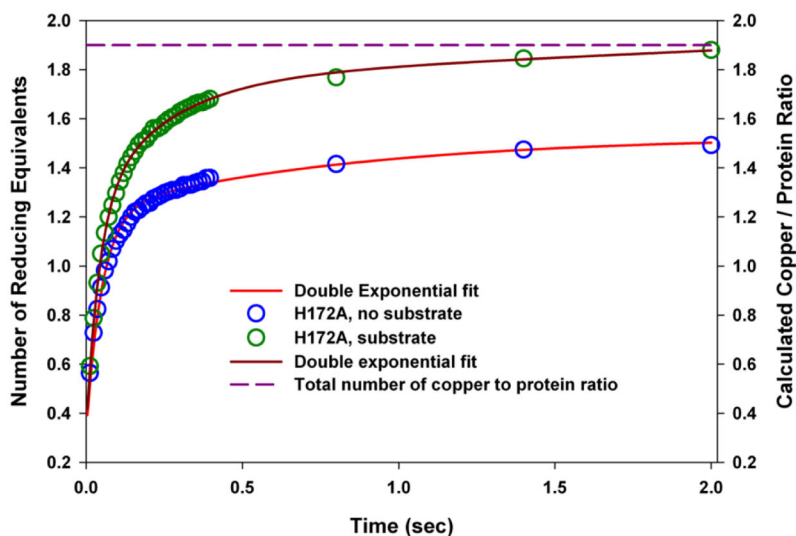
Figure 6.
Stopped-flow reduction kinetic traces of the H172A mutant (0–2 seconds) in the absence of substrate Ac-YVG (open blue circles) fitted to a double exponential (red line) and in presence of the substrate Ac-YVG (open green circles) fitted to a double exponential (brown line). The purple dashed line represents the total copper to protein ratio in the H172A sample. The kinetic parameters used for the fits are listed in Table 1. Note: The split time-base used to capture the end point of the slower phase results in fewer time points after 400 ms.
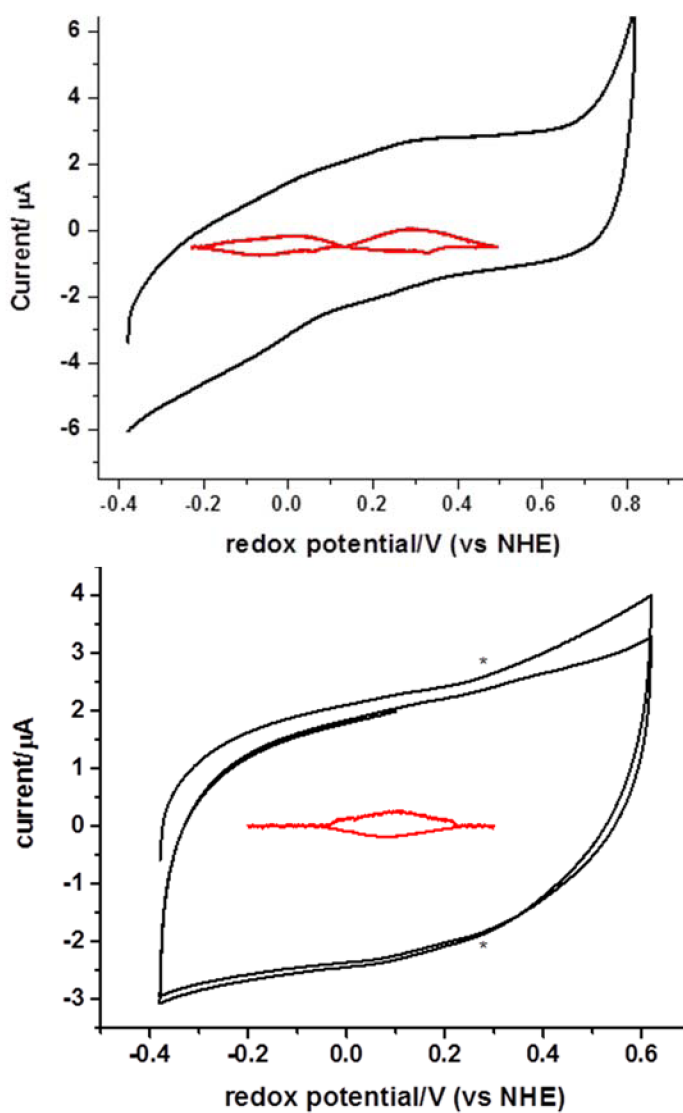
Figure 7.
Reversible behavior of the PHM Cu(II)/Cu(I) redox couple in the absence (top) and presence (bottom) of Ac-YVG substrate. Voltammagrams were measured in 50 mM MES, pH= 6.0 + 100 mM NaCl, on ice, and under Ar flow. The scan rate in all cases was 250 mV/s. (black line). The signal with the capacitive current subtracted is shown as an inset in the middle (red line). E_m values are listed in Table 2.
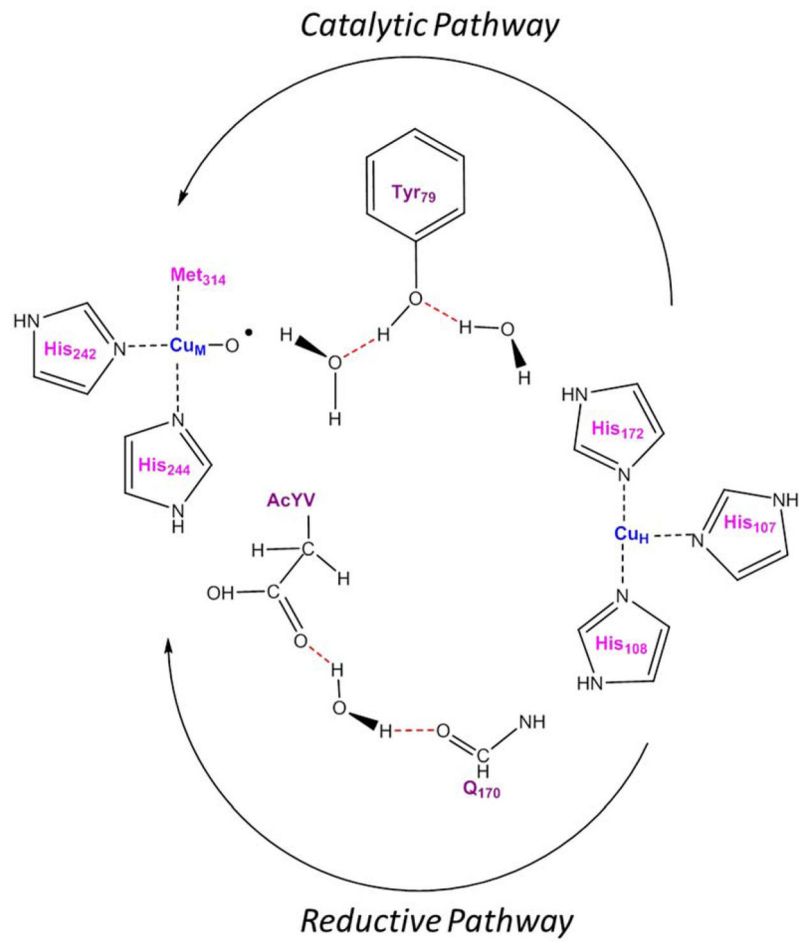
Figure 8.
Proposed bifurcated ET pathways for the reductive and catalytic electron transfer steps.

Table 1

Rate constants for reduction of WT PHM and its variants in the absence and presence of substrates

Sample	Cu-H[a] amplitude	Cu-H Rate (s^{-1})	Cu-M[a] amplitude	Cu-M Rate (s^{-1})
No Substrate				
WT PHM	1.1	17.2(6)[b]	1.0	0.5(1)
H242A	0.7	42.5(10)		
H107AH108A			0.7	0.026(5)
H108A	0.6	40.3(8)		
H172A	0.9	19.8(8)	0.3	1.2(9)
With Substrate				
WT-AcYVG	1.1	30.7(19)	1.1	4.2(3)
WT-nitrohippurate	0.9	37.5(13)	1.1	2.8(2)
WT-hippurate	0.7	9.7(11)	1.1	2.0(5)
H242A-AcYVG	0.7	26.3(1)		
H107AH108A-AcYVG	0.6		0.6	0.025(1)
H108A-AcYVG	0.7	38.9(7)		
H172A-AcYVG	0.9	24.0(4)	0.6	4.1(1)

[a]Values of the amplitude of each exponential are related to the site occupancy of H and M sites. They were initially floated to determine approximate values and then fixed in subsequent iterations of the non-linear regression analysis.

[b]Numbers in parentheses represent the standard deviation in the preceding value. Thus 17.2(6) represents 17.2 ± 0.6 while 42.5(10) represents 42.5 ± 1.0.

Table 2

E_m values (vs NHE) for WT PHM and its variants at pH 6.0

Sample	E_m (mV)	Standard deviation
WT-peak 1	−15	8
WT-peak 2	270	5
WT + AcYVG	83	18
H242A	213	5
H107AH108A	140	2
H108A	270	1
H172A	**(210)**[a]	Poorly defined

[a] This mutant was poorly behaved on the electrode and probably unfolded. This value therefore represents an estimate with a large undefined error.